analytical chemistry

Article

pubs.acs.org/ac

# Amperometric Noise at Thin Film Band Electrodes

Simon T. Larsen,[†] Michael L. Heien,[‡] and Rafael Taboryski*,[†]

[†]Department of Micro- and Nanotechnology, Technical University of Denmark, DTU Nanotech, Building 345B, DK-2800 Kongens Lyngby, Denmark

[‡]Department of Chemistry and Biochemistry, University of Arizona, 1306 E. University Blvd., Tucson, Arizona 85721, United States

**ABSTRACT:** Background current noise is often a significant limitation when using constant-potential amperometry for biosensor application such as amperometric recordings of transmitter release from single cells through exocytosis. In this paper, we fabricated thin-film electrodes of gold and conductive polymers and measured the current noise in physiological buffer solution for a wide range of different electrode areas. The noise measurements could be modeled by an analytical expression, representing the electrochemical cell as a resistor and capacitor in series. The studies revealed three domains; for electrodes with low capacitance, the amplifier noise dominated, for electrodes with large capacitances, the noise from the resistance of the electrochemical cell was dominant, while in the intermediate region, the current noise scaled with electrode capacitance. The experimental results and the model presented here can be used for choosing an electrode material and dimensions and when designing chip-based devices for low-noise current measurements.

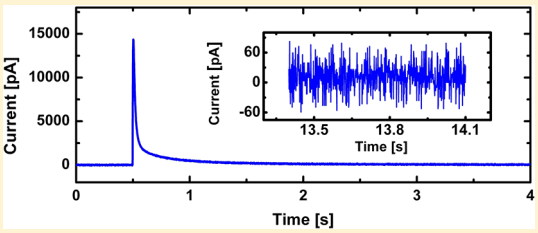


Electrochemical detection using constant-potential amperometry is a widely used technique in biosensor applications. Many biologically interesting molecules are electroactive and can thus be oxidized at an electrode held at a sufficient positive potential. Amperometric detection is used in applications such as capillary electrophoresis,[1,2] high performance liquid chromatography,[3] and measurements of neurotransmitter released from living cells.[4] Electrical background noise is one of the major limitations of amperometric detection defining the limit for the smallest possible detectable signals. The signal-to-noise ratio is often used to quantify the precision of amperometric data.

Microelectrodes coupled with low-noise amplifiers have been used to measure currents with noise levels down to the femtoampere region.[5] Traditionally, carbon-fiber microelectrodes have received the most attention due to their excellent low-noise properties, but in the past decade, much research has focused on developing thin-film microelectrodes from different electrode materials for amperometric detection using chip-based devices. These materials include gold,[6,7] platinum,[8] indium tin oxide,[9] pyrolyzed photoresist,[10] diamond-like carbon,[11] and conductive polymers like Pedot:Pss[12] and Pedot:tosylate.[13]

Current noise is generally measured in terms of the root-mean-square of the current. General theories on current noise in electrochemical detectors covering also faradaic currents have been presented.[14−17] In constant potential amperometric recordings of exocytosis, the faradaic signal only gives rise to small current transients and the major noise concern is typically associated with the background noise of the electrode resulting from nonfaradaic interactions between the electrode and the physiological salt buffer.[18−21] This amperometric background noise is often thought of as being proportional to electrode capacitance and hence electrode area.[22−24] For carbon fiber-microelectrodes, this was shown to be the case except for very small electrodes where the amplifier noise became predominant.[18] The proportionality between the root-mean-square noise and the electrode area was also demonstrated for thin-film electrodes made of gold[19] and indium tin oxide.[20,21] For Pedot:Pss conductive polymer microelectrodes, larger electrodes were shown to be more noisy,[12] while for micrometer-sized platinum electrodes, the current noise was indistinguishable from amplifier noise in the open loop configuration.[8]

In this paper, we present extensive amperometric noise data for thin-film microelectrodes held at a constant potential in a physiological buffer. The experimental setup and the measurement parameters correspond to those used in typical low-noise amperometric measurements of exocytosis from single cells. Electrodes were made of gold and conductive polymers Pedot:Pss and Pedot:tosylate. These materials differ widely in capacitive properties, allowing for the analysis of noise behavior for a wide range of electrode capacitances. In addition, we present a simple and adequate noise expression, depending only on the electrode capacitance, the resistance of the cell, the filter frequency, and the open loop amplifier noise. Experimental data strongly supports the analytical solution. We find that the noise scales with the electrode capacitance except for very small capacitances where the potentiostat noise dominates and for sufficiently large capacitances where the noise is equal to the Johnson−Nyquist noise of the circuit resistance. The dependence of the noise on circuit resistance is also modeled. Limits for the different noise regimes are reported, and some

**Received:** April 30, 2012
**Accepted:** August 28, 2012
**Published:** August 28, 2012

 © 2012 American Chemical Society  dx.doi.org/10.1021/ac301136x | *Anal. Chem.* 2012, 84, 7744−7749

practical suggestions are provided for designing thin-film microelectrodes for low-noise amperometry applications.

## MATERIALS AND METHODS

Pedot:tosylate band microelectrodes were fabricated on polymer (TOPAS) substrates as described earlier.[13] Pedot:Pss band electrodes were prepared by spin-coating Pedot:Pss aqueous solution (483095, Sigma-Aldrich) at 1000 rpm for 30 s onto polymer (TOPAS) substrates. Pedot:Pss samples were subsequently covered with 70% dimethylsulfoxide (DMSO, >99% purity, Merck, Germany) in water, heated at 70 °C for 5 min, and washed in deionized water. Patterning of the Pedot:Pss layer was done as described earlier for Pedot:tosylate microelectrodes.[13]

Gold microelectrodes were fabricated on 4 in. Boron glass wafers. The glass wafers were placed overnight in a 250 °C oven and then silylated with hexamethyldisilazane (HMDS). A 1.5 $\mu$m layer of AZ5214E photoresist was spin-coated on the glass wafers. The samples were baked at 90 °C for 60 s before being exposed in a Karl Suss MA6/BA6Mask Aligner for 6 s (intensity 7.0 mW/cm$^2$) and developed with AZ351B Developer. The photomask was ordered at Delta Mask B.V. Residual resist was removed with a Plasma Asher (TePla). A Wordentec QCL800 Metal evaporator was used to first evaporate a 5 nm adhesion layer of chrome (1 n/s, 5 s) and then 150 nm of gold (1 n/s, 150s). Finally, resist was lifted off in acetone, and the electrode substrates were rinsed with isopropanol and water and dried. For all electrode materials, electrodes between 3 and 50 $\mu$m wide and 6 mm long were fabricated.

Electrochemical noise measurements were made using an Axopatch 200B (Molecular Devices) amplifier. The resistive feedback configuration was used. In order not to limit the measurement bandwidth, we worked with the lower feedback resistance option of the Axopatch, $R_f$ = 50 MΩ, while low-pass filtering at 1 kHz using the 4 pole Bessel filter of the amplifier. The gain used was 20 mV/pA for noise measurements, but in general, the noise did not depend on the gain unless a very low gain was used. A PDMS well was fabricated and bonded to an electrode surface. The band electrode protruded into the bonded PDMS well which was filled with PBS buffer (phosphate-buffered saline, Sigma Aldrich). The electrode length depended on the penetration depth into the well, and it was measured using a microscope. A Ag/AgCl reference electrode (RE-5B, BASi) was placed with the tip in the PDMS well and connected to the amplifier headstage. Connections to the working electrode were made using conductive epoxy glue (Conductive Epoxy, Chemtronics).

Current data was collected using an amperometry program written in LabVIEW (National Instruments, Austin, Texas). The voltage was applied at the Axopatch 200b amplifier. For each noise measurement, five short noise traces were measured, and the average of the offset corrected root-mean-square of the current was used to describe the magnitude of the noise. Conductivity was measured with a four-point probe (Jandel Engineering Ltd.) connected to a Keithley 2400 SourceMeter (Keithley Instruments Inc.).

The uncertainty of experimental noise data was estimated by using the uncertainties of capacitance, resistance, and open loop current noise values and calculating the propagated error of the theoretical value for the same parameters. For discrete resistors and capacitors, the uncertainty was provided by the manufacturer to be 5% for resistors and 20% for capacitors. For electrodes, the capacitance uncertainty was dominated by the uncertainty in area estimation using optical microscopy.

## RESULTS AND DISCUSSION

All noise measurements were carried out using an Axopatch 200B amplifier connected to an electrochemical cell corresponding to the one depicted in Figure 1a. Thin-film band electrodes were fabricated on either glass or polymer substrates, and active areas were defined by bonding the substrates to PDMS wells. After bonding, the exact electrode area could be determined by microscopic observation. Noise traces were recorded after applying a constant voltage (100 mV) to the electrochemical cell and waiting until the current had decayed to approximately zero (Figure 1b). Interference noise from 50 Hz noise sources was avoided by shielding with two separate faraday cages, an outer cage held at earth ground and an inner cage connected to signal ground from the amplifier. The noise was low pass filtered at 1 kHz using the 4 pole Bessel filter of the Axopatch 200B amplifier. This frequency is within the range of filter frequencies typically used for amperometric exocytosis measurements at single cells.[25,26]

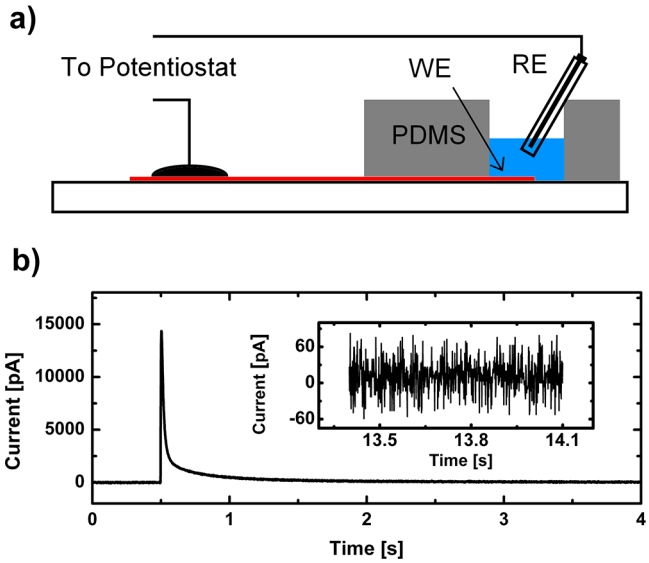


**Figure 1.** (a) Electrochemical setup. The active working electrode (WE) is defined by the area of a thin film band electrode (red) protruding into a well made of PDMS. The reference electrode (RE) is placed in the buffer solution (PBS). (b) Current response following a voltage step (0 to 100 mV) at a Pedot:tosylate microelectrode. The inserted graph is showing the noisy current trace at a later time where the current has reached a constant value.

The noise model used in this work is based on the simplified equivalent circuit shown in Figure 2. Here, the electrode is represented as a perfect capacitor while the solution resistance

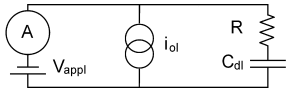


**Figure 2.** Simple equivalent circuit for electrochemical cell. $V_{appl}$ is the applied potential, $C_{dl}$ is the double-layer capacitance of the electrode, $R$ is the sum of resistances in series with the electrode, and $i_{ol}$ is the open-loop current noise represented as a current source in parallel with the cell.


dx.doi.org/10.1021/ac301136x | Anal. Chem. 2012, 84, 7744−7749

of the buffer and the resistance of wires and isolated electrode connections is represented by a resistor with resistance $R$. The current noise measured at an open loop configuration is represented as a current source in parallel with the cell. This noise is a measurable quantity and may, except for operational amplifier noise of the headstage, also include microphonic noise in cables or possibly interference noise from nonefficient shielding. Other noise sources of practical nature like noise in liquid junctions are assumed to play a minor role compared to intrinsic voltage noise of the circuit and therefore are neglected.

We describe the total current power spectral density $S_i$ as the sum of power spectral densities from uncorrelated random noise sources. Shot noise has been disregarded as a noise source since the background current in our experiment is close to zero. This leaves the open loop current noise $I_{RMS,ol}$ with power spectral density $S_{i,ol}$ as well as current noise from ohmic behavior of voltage noise sources. Since in this work we are interested in microfabricated thin film electrodes where isolated electrode segments and the buffer solution typically give rise to series resistances above $10^4$ Ω, the Johnson−Nyquist noise from $R$ is the main contribution of voltage noise. Since the current noise is given by the voltage noise divided by the impedance, we write the total power spectral density of the current noise as

$$S_i(f) = \frac{4kTR}{R^2 + \frac{1}{(2\pi fC)^2}} + S_{i,ol}(f) \quad (1)$$

where $k$ is Boltzmann's constant ($1.38 \times 10^{-23}$ J/K), $T$ is the absolute temperature, and $f$ is the frequency in Hz. The interesting experimental noise parameter is the root-mean-square of the current trace. The current trace is typically filtered with a low-pass active analog filter with cutoff frequency $f_c$. Assuming the low-pass filter is ideal, i.e., all signals below $f_c$ pass and all signals above $f_c$ are stopped, the root-mean-square current noise can be found by integrating the power spectral density from $f = 0$ to $f = f_c$.

$$I_{RMS}^2 = \int_0^{f_c} S_i(f)\, df \quad (2)$$

Integrating eq 1, we obtain:

$$I_{RMS}^2 = \frac{4kT}{R}\left(f_c - \frac{1}{2\pi RC}\,\mathrm{Arc\,tan}(2\pi RCf_c)\right) + I_{RMS,ol}^2 \quad (3)$$

Here, $I_{RMS,ol}$ is the root-mean-square current noise of the headstage in an open loop configuration.

For real low-pass filters, the cutoff is not sharp but extends over a range of frequencies. Therefore a more accurate estimate for the root-mean-square current noise is found by multiplying the power spectral density of the unfiltered input by the square of the filter transfer function's magnitude response $|H(j\omega)|$ before integration.

$$I_{RMS}^2 = \int_0^{\infty} |H(j\omega)|^2 S_i(f)\, df \quad (4)$$

where $j$ is the imaginary unit and $\omega = 2\pi f$ the angular frequency. Transfer functions can be rather complicated mathematical functions, which makes eq 4 better suited for numerical integration than analytical evaluation.

In this paper, we used the analog 4 pole Bessel filter of the Axopatch 200B amplifier for noise measurements. The filter cutoff frequency was held at 1 kHz for all measurements. The open loop root-mean-square current noise was measured before each experiment. It was typically around 0.7 pA in the measurement bandwidth. (The relatively high open loop noise is due to choice of feedback element on the Axopatch amplifier. The lower (and noisier) feedback resistor (50 MΩ) was chosen in order to get a larger output bandwidth of the probe.) This leaves only two unknown quantities in eqs 1 and 3, the electrode capacitance and the resistance in series.

First, we test our model by replacing the electrochemical cell by discrete resistors and capacitors. The blue line in Figure 3 shows the measured power spectral density of the current noise, when using a 1 nF capacitor and a 100 kΩ resistor in series. The dashed black line shows the calculated power spectral density using eq 1. The noise power is plotted as $pA^2$/Hz, and the open loop noise is neglected in this example since it is much lower than the Johnson−Nyquist noise from the resistor. Assuming an ideal filter with cutoff at 1 kHz, the filtered power spectral density would correspond to the solid black line and the root-mean-square noise would be equal to the integral of this. Taking into account the 4 pole Bessel filter and multiplying the power spectral density with the square of the filter transfer function's magnitude response $|H(j\omega)|$,[27] a better estimate of the power spectral density can be found (red line, Figure 3). It should be noted that the choice of resistor and capacitor in this example was made to illustrate the difference between using eqs 2 and 4. In most cases, the difference in root-mean-square currents calculated by taking the Bessel filter transfer function into account or using the simpler analytical solution for an ideal filter is less pronounced than in Figure 3.

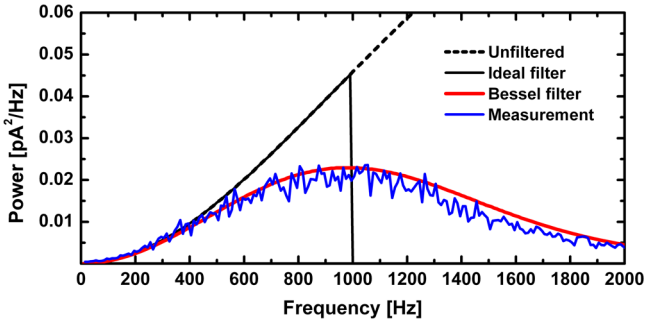


**Figure 3.** Measured power spectral density of the current noise for a 1 nF capacitor and a 100 kΩ resistor in series held at 100 mV and low-pass filtered at 1 kHz through an analog 4 pole Bessel filter at an Axopatch 200B amplifier (blue) plotted along with theoretical plots for ideally filtered and 4 pole Bessel filtered power spectral densities.

In Figure 4, we show measured root-mean-square current noise values for a wide range of different resistors and capacitors. Five short noise traces were measured for each configuration, and the average of the offset corrected root-mean-square current noise was plotted. Along with experimental values, theoretical curves are plotted corresponding to root-mean-square current noise values calculated using eqs 3 and 4. Clearly, the theoretically calculated values fit the measured values nicely. This indicates that eqs 3 and 4 can describe current noise at electrodes if the equivalent circuit of the electrochemical cell can be described as a resistor and capacitor in series. As expected, taking the Bessel filter behavior into account, the best match with experiments is obtained, but also the simpler analytical solution of eq 3 describes the noise very well.


dx.doi.org/10.1021/ac301136x | Anal. Chem. 2012, 84, 7744−7749

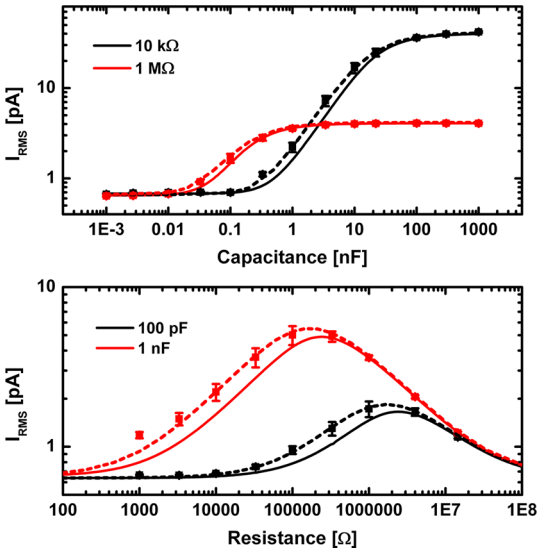


**Figure 4.** The root-mean-square current noise values for sets of discrete resistors and capacitors in series. Capacitance is varied in the upper graph while resistance is varied in the lower graph. Solid lines show calculated noise values corresponding to eq 3. Dashed lines show noise values calculated by numerical integration of eq 4. (Filter frequency: 1 kHz, $I_{RMS,ol}$ = 0.65 pA.)

Observing the noise behavior in Figure 4, we notice three domains; the noise is constant for (1) very low or (2) very large capacitances. At lower capacitances, the open loop current noise dominates completely, while at the large capacitances, the noise is equal to the Johnson−Nyquist noise from the resistor, meaning the capacitance has no effect on the noise (3). In the intermediate region, the root-mean-square scales with capacitance. Indeed, for small capacitances, using the two first terms of the Arctan Taylor expansion, eq 3 becomes

$$I_{RMS}{}^2 = \frac{4}{3}kTR(2\pi C)^2 f_c{}^3 + I_{RMS,ol}{}^2 \quad (5)$$

Equation 5 fits the measured noise values shown in Figure 4 corresponding to low and intermediate capacitances. As long as the open loop noise has no effect, the root-mean-square current noise is directly proportional to the capacitance. Since the capacitance of an electrode is generally proportional to the electrode area, the root-mean-square noise is proportional to area. This result is in agreement with literature on the subject of microelectrode noise (vide supra). The criterion for being in the large capacitance region is that resistance dominates the total cell impedance, i.e., $R^2 \gg 1/(2\pi fC)^2$ . Oppositely, if capacitance dominates the impedance, noise scales with capacitance until amplifier noise become dominant.

Varying the resistance results in peak-shaped noise curves (Figure 4). For very large resistances, the current noise decreases, but for these values, the time constant of the electrochemical cell $\tau = RC$ also increases. This is an unwanted side effect for fast sampling experiments. Reducing the resistance is often the best approach although this can be difficult in chip-based devices, where solution resistance in microfluidic channels is often significant.

In the experimental work presented here, we limit our noise investigation to variations in cell resistance and capacitance. This is due to the fact that the two other variables in eq 3, the open loop amplifier noise and the low pass cutoff filter frequency, have a much simpler effect on the noise. As mentioned above, the open loop amplifier noise just determines the noise level for very low capacitances. For the filter cutoff frequency, noise increases with increasing frequency except for very low capacitances.

Next, we turn our attention to real electrodes. If the electrochemical cell can be described by a capacitor and resistor in series, the model presented here should apply to the current noise. As mentioned above, the capacitance of an electrode is generally proportional to the electrode area. It can be described by the expression

$$C = \left(\frac{C}{A}\right)_i A \quad (6)$$

where the capacitance per area $(C/A)_i$ is a constant depending on the electrode material. In this work, we find $(C/A)_i$ for each electrode material by measuring the capacitance of a large electrode and dividing it by the area. The apparent capacitance is found by dividing the charging current measured at a cyclic voltammogram by the scan rate. Although this method is based on a simplification since capacitance can also be a function of voltage and scan rate, it is an appropriate estimate of the electrode capacitance for many electrodes. Substituting $C$ in eq 3 by the above expression (eq 6) gives us a noise theory depending on electrode area and series resistance of the electrode.

Estimating the series resistance of an electrode system is more difficult, since it depends on both electrode connections and the resistance of the solution. In chip-based devices, the working electrode is typically connected to the potentiostat by an electrode segment isolated by the substrate and the bonded counterpart as shown in Figure 1a. For a band electrode of length $l$ and width $w$, the resistance of this wire is given by

$$R = R_s\frac{l}{w} \quad (7)$$

where $R_s$ is the sheet resistance of the film. For metal electrodes, the resistance of isolated electrode connections is typically negligible compared to other resistance sources, but for electrodes made of materials with higher resistivity like conductive polymers or pyrolyzed photoresist, this resistance can be significant.

The solution resistance which makes up another significant part of the total resistance is generally thought to be inversely proportional to electrode radius for disk microelectrodes.[28,29] Assuming spherical symmetry around the microelectrode, this resistance could be described by the equation

$$R_u = \frac{1}{4\pi\kappa r_0} \quad (8)$$

Here, $\kappa$ is the conductivity of the solution and $r_0$ is the radius of the disk microelectrode. For the band electrodes used in this work, eq 6 does not apply directly since we have neither spherical symmetry nor disk shaped electrodes. It is reasonable though to assume the solution resistance to be inversely proportional to a critical electrode dimension. If we assume this dimension to be the length of the band electrode, the total resistance of the electrochemical cell can be expressed as

$$R = R_{el} + \frac{k_s}{l} \quad (9)$$

Here, the first tem $R_{el}$ is the resistance of isolated parts of the electrode (and wires), $k_s$ is a constant depending on the buffer


dx.doi.org/10.1021/ac301136x | Anal. Chem. 2012, 84, 7744−7749

solution and placement of the reference electrode, and $l$ is the electrode length.

In order to test the applicability of our theory on real electrodes, we first connected a large discrete resistor (330 kΩ) in series with different band electrodes, while keeping electrode connections short and the reference electrode close to the band electrodes. The discrete resistor dominates the total resistance making the measurements easier to compare to theory. Figure 5

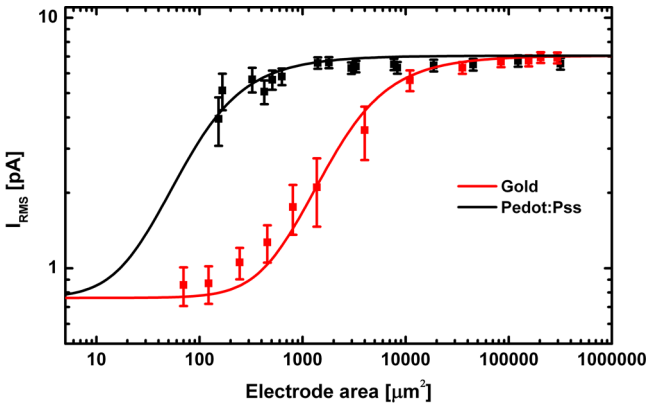


**Figure 5.** Measured current noise values as a function of electrode area at gold and Pedot:Pss electrodes. A large external resistor (330 kΩ) was connected in series with the electrodes to give a dominate resistance. Solid lines show expected theoretical noise values given by eq 3.

shows noise results for Pedot:Pss and gold electrodes varying in area between 100 and 10000 $\mu m^2$. The noise at gold electrodes is clearly smaller than the noise at Pedot:Pss electrodes. Using cyclic voltammetry, we measured the apparent capacitance per area of the electrodes (Table 1). Using these values and eqs 3

**Table 1. Capacitance per Area and Sheet Resistance for Electrodes Used for Noise Measurements**

| | | |
|---|---|---|
| gold | 18.6 ± 2.0 $\mu F/cm^2$ | 0.185 Ω ± 0.005 Ω |
| Pedot:Pss | 460 ± 60 $\mu F/cm^2$ | 3200 Ω ± 200 Ω |
| Pedot:tosylate | 1700 ± 100 $\mu F/cm^2$ | 580 Ω ± 70 Ω |

and 6, we now plot the theoretical electrode noise as a function of area (solid lines, Figure 5). Clearly, the theory fits the experimental data well. The large difference in capacitance properties between Pedot:Pss and gold is reflected in the displacement of the two graphs along the $x$-axis. Much smaller capacitance Pedot:Pss electrodes are needed to achieve the same low noise as that at gold electrodes.

Finally, we present noise measurements from electrodes with no external resistor connected. The setup is as shown in Figure 1a. The electrode capacitance is still given by eq 6, while the resistance is now coming only from the isolated electrode segments and the solution. In Figure 6, we show noise results for Pedot:tosylate and gold electrodes. The area of the electrode is varied by shortening the length of the electrode protruding into the PDMS well. Equation 3 is used to fit the experimental noise data. The expressions for resistance and capacitance given by eqs 6 and 9 are used, and least-squares fitting (we used an excel spreadsheet with the data points and the theory in different columns, made a third column with squares of errors, and minimized the sum of this column using the Solver function) is done using $R_{el}$ and $k_s$ as fitting

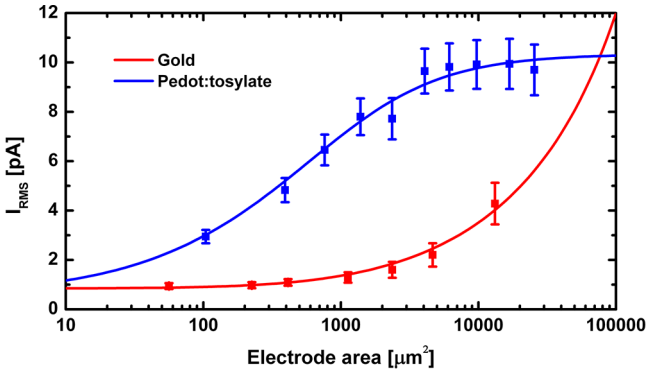


**Figure 6.** Current noise measurements at gold and Pedot:tosylate band electrodes. Solid lines show theoretical noise obtained by least-squares fitting of eq 3.

parameters. Resulting fits are in good agreement with experimental values and are shown as solid lines in Figure 6. The least-squares fitting resulted in the following parameters: $R_{el}$ = 439 Ω and $k_s$ = 41.8 Ω × m for gold and $R_{el}$ = 152 000 Ω and $k_s$ = 35.6 Ω × m for Pedot:tosylate. Since the same reference electrode and buffer solution is used for both electrodes, it is expected that the fitted $k_s$-values do not differ much. Further, the $R_{el}$ values are also realistic and reflect the large difference in sheet resistance for thin films of gold and Pedot:tosylate (table 1). Indeed, if the dimensions of the electrode connections used in this experiment (3.75 $\mu$m × 2900 $\mu$m for gold and 4.6 $\mu$m × 900 $\mu$m for Pedot:tosylate) are used together with eq 7 and the sheet resistance values of Table 1, calculated electrode connection resistances are 143 Ω for gold and 114000 Ω for Pedot:tosylate. These values are in the same order of magnitude as the fit $R_{el}$-values.

A few practical points can be made in relation to the electrode noise measurements presented here. First, for low noise current amperometry, the choice of electrode material is important. As seen in Figure 6, Pedot:tosylate electrodes had to be made almost 2 orders of magnitude smaller than gold electrodes to reach the same noise level. Second, the resistance of electrode wires and the solution resistance in microfluidic channels also affect the noise. If this resistance dominates the impedance of the electrochemical cell, the noise is equal to the Johnson−Nyquist noise of the resistance as seen for the large Pedot:tosylate electrodes in Figure 6. In this regime, the noise decreases for increasing resistance but simultaneously the time constant increases, making the system more sluggish.

## CONCLUSION

In this work, we presented an analytical solution for the current noise at microelectrodes during constant potential amperometry experiments such as amperometric recordings of transmitter release events from single cells. Thin-film band microelectrodes were fabricated in three different electrode materials with different capacitive properties, and current noise was measured for a wide range of different electrode areas. The results agreed very well with the analytical noise expression. Our results emphasize the importance of choosing low capacitive electrode materials and small electrodes if low current noise is crucial. We observed three different noise regimes. (1) For very low capacitances, the noise was equal to the open loop noise of the potentiostat. (2) For very large capacitances, the noise was equal to the Johnson−Nyquist noise of the resistance of the electrochemical cell. (3) In the


dx.doi.org/10.1021/ac301136x | Anal. Chem. 2012, 84, 7744−7749

intermediate region, noise scaled with capacitance. The noise expression presented here could be used for designing chip-based devices with integrated microelectrodes for low-noise amperometric sensing

## AUTHOR INFORMATION


### Corresponding Author

*E-mail: rata@nanotech.dtu.dk.


### Notes

The authors declare no competing financial interest.

## ACKNOWLEDGMENTS

This work is supported by the Danish Council for Strategic Research through the Strategic Research Center PolyNano (grant no. 10-092322/DSF).

## REFERENCES


(1) Ge, S.; Koseoglu, S.; Haynes, C. L. *Anal. Bioanal. Chem.* **2010**, *397*, 3281−3304.
(2) Vandaveer, W.; Pasas-Farmer, S.; Fischer, D.; Frankenfeld, C.; Lunte, S. *Electrophoresis* **2004**, *25*, 3528−3549.
(3) Lavrik, N. V.; Taylor, L. T.; Sepaniak, M. J. *Anal. Chim. Acta* **2011**, *694*, 6−20.
(4) Omiatek, D. M.; Cans, A.; Heien, M. L.; Ewing, A. G. *Anal. Bioanal. Chem.* **2010**, *397*, 3269−3279.
(5) Wightman, R.; Jankowski, J.; Kennedy, R.; Kawaoge, K.; Schroeder, T.; Leszczyszyn, D.; Near, J.; Diliberto, E.; Viveros, O. *Proc. Natl. Acad. Sci. U.S.A.* **1991**, *88*, 10754−10758.
(6) Spegel, C.; Heiskanen, A.; Pedersen, S.; Emneus, J.; Ruzgas, T.; Taboryski, R. *Lab Chip* **2008**, *8*, 323−329.
(7) Dittami, G. M.; Rabbitt, R. D. *Lab Chip* **2010**, *10*, 30−35.
(8) Berberian, K.; Kisler, K.; Fang, Q.; Lindau, M. *Anal. Chem.* **2009**, *81*, 8734−8740.
(9) Amatore, C.; Arbault, S.; Chen, Y.; Crozatier, C.; Lemaitre, F.; Verchier, Y. *Angew. Chem., Int. Ed.* **2006**, *45*, 4000−4003.
(10) Hebert, N.; Snyder, B.; McCreery, R.; Kuhr, W.; Brazill, S. *Anal. Chem.* **2003**, *75*, 4265−4271.
(11) Gao, Y.; Chen, X.; Gupta, S.; Gillis, K. D.; Gangopadhyay, S. *Biomed. Microdevices* **2008**, *10*, 623−629.
(12) Yang, S. Y.; Kim, B. N.; Zakhidov, A. A.; Taylor, P. G.; Lee, J.; Ober, C. K.; Lindau, M.; Malliaras, G. G. *Adv. Mater.* **2011**, *23*, H184−H188.
(13) Larsen, S. T.; Vreeland, R. F.; Heien, M. L.; Taboryski, R. *Analyst* **2012**, *137*, 1831−1836.
(14) Morgan, D.; Weber, S. *Anal. Chem.* **1984**, *56*, 2560−2567.
(15) Hassibi, A.; Navid, R.; Dutton, R.; Lee, T. *J. Appl. Phys.* **2005**, *98*, 069903.
(16) Weber, S. *Anal. Chem.* **1989**, *61*, 295−302.
(17) Wiedemann, D.; Kawagoe, K.; Kennedy, R.; Ciolkowski, E.; Wightman, R. *Anal. Chem.* **1991**, *63*, 2965−2970.
(18) Schulte, A.; Chow, R. *Anal. Chem.* **1998**, *70*, 985−990.
(19) Chen, P.; Xu, B.; Tokranova, N.; Feng, X.; Castracane, J.; Gillis, K. *Anal. Chem.* **2003**, *75*, 518−524.
(20) Sun, X.; Gillis, K. *Anal. Chem.* **2006**, *78*, 2521−2525.
(21) Meunier, A.; Fulcrand, R.; Darchen, F.; Collignon, M. G.; Lemaitre, F.; Amatore, C. *Biophys. Chem.* **2012**, *162*, 14−21.
(22) Hochstetler, S.; Puopolo, M.; Gustincich, S.; Raviola, E.; Wightman, R. *Anal. Chem.* **2000**, *72*, 489−496.
(23) Long, J.; Weber, S. *Anal. Chem.* **1988**, *60*, 2309−2311.
(24) Li, Z.; Zhou, W.; Wu, Z.; Zhang, R.; Xu, T. *Biosens. Bioelectron.* **2009**, *24*, 1358−1364.
(25) Hafez, I.; Kisler, K.; Berberian, K.; Dernick, G.; Valero, V.; Yong, M.; Craighead, H.; Lindau, M. *Proc. Natl. Acad. Sci. U.S.A.* **2005**, *102*, 13879−13884.
(26) Liu, X.; Barizuddin, S.; Shin, W.; Mathai, C. J.; Gangopadhyay, S.; Gillis, K. D. *Anal. Chem.* **2011**, *83*, 2445−2451.
(27) Winder, S. *Analog and Digital Filter Design*, 2nd ed.; Newnes: Amsterdam, 2002.
(28) Bard, A. J.; Faulkner, L. R. *Electrochemical Methods*, ed.; John Wiley & Sons, Inc.: Hoboken, NJ, 2001.
(29) Zoski, C. G., Ed. *Handbook of Electrochemistry*; Elsevier: Amsterdam, 2007.